StrucOpt manuscript No.
(will be inserted by the editor)

Why grain in tree's trunks spiral: mechanical perspective

Seubpong Leelavanichkul and Andrej Cherkaev

Abstract In the present work, the specific question as to whether the optimization of the spiral grain of trees can be described from the mechanical point of view is addressed. Computations of stresses and the optimized grain angle using the theory of anisotropic elasticity are reported, along with the comparison to the actual data of Ponderosa pine. The results show good agreement between the computed and the measured grain angle. If the structure of the tree is optimized for the strength, spiraling of the grain does not lower this requirement. At the same time, fluid is allowed to be transported across the circumference of the trunk. To have a clear understand why the tree spirals, other factors and approaches should supplement the present analysis.

Key words Spiral grain, Anisotropic elasticity, Wood failure, Biomimetics

Fig. 1 Ponderosa pine (photo by Cherkaev).

1 Introduction

The paper concerns with explanation of morphology of tree's trunk from structural optimization viewpoint. Specifically, we investigate reasons behind spiral grows of tree's trunk in Ponderosa Pine in South Utah. These trees develop helicoidal wood fibers that wiggle around the trunk as spirals. Spiral grain can be seen on many trees; they are visible when the bark is removed from the trunk; the angle is about $30° - 50°$. The questions that have often been asked are why do they twist, what direction do they twist, and how much do they twist? (Figure 1). The paper performs stress analysis to answer the question: Why the grain in the trunks of many trees twists.

Many different reasons and hypotheses have been made and primarily among them are the earth rotation, the wind, and even the gravitational effect of the moon (Gedney (1986)). According to the work done by Kubler (1991), the spiral growth allows water from each individual root to reach every branch on the tree. In addition, trees become less stiff and bend more easily because of the spiral grain. This bending allows trees to become more effective at discarding excessive snow from their branches and more resistant to breakage from heavy winds. Kubler (1991) also found that spiral grain is often seen on trees at the dry rocky site. In theory, tree branches with straight grain are fed only by those roots directly below them. If the roots on either side of the tree are cut, then straight grain branches on that side will die. In comparison, each root of a spiral grain tree feeds nearly the whole tree. If all the roots on one side die, that side of the tree will still be healthy. The reason for this is the xylem. Xylem is the tissue in a vascular plant, consisting of woody fibers, tracheid, and parenchymatous cells, through which water passed upward from roots, and which provides support for the plant. The xylem spirals less around the stem as the tree grows and the stem diameter increases. When the tree grows each year, the growth is slightly

Received: date / Revised version: date

Seubpong Leelavanichkul and Andrej Cherkaev

Department of Mathematics, University of Utah, Salt Lake City, UT 84112 USA

offset from previous years. Hence, the flow from one root is distributed almost completely around the tree bole. This has been proven by injecting conifers with dye at the base. As conditions get harsher, the grain tends to spiral at a more extreme angle around the stem. This qualitative analysis, however, does not answer the question: how large is the angle?

There may be also a good mechanical reason behind this development of the trunk. Studying morphologies like bones or trunks which are critical for the survival of a species, we may postulate that they are optimally adapted to the environment. We should agree that trunks of trees should stay unbroken and they should be able to sustain extreme dynamic loads applied from all directions when a strong wind bends a tree.

We suppose that spiraling grains around a trunk is a more complicated structure than a structure of straight vertical grains. If a natural 'design' becomes more complex, there must be a reason for this. Understanding the nature of optimality helps to incorporate the same concept into the design of a similar engineering structure (biomimetics). We use methods of structural optimization to discuss the spiral in the tree. The selected biological structure performs a clearly defined mechanical task, the acting forces are known, the model is relatively simple, and the data on the morphology is available. A systematic mathematical technique is needed for the search of a goal functional of an optimization problem with a known solution; this technique could be called "reverse optimization:" it is aimed to explain the adaptation of bio-structures. Here we use a simplified approach to the problem: Choosing the goal functional from several of independently guessed hypotheses.

Notice that the optimization problems in engineering and in biology are mutually reciprocal. The biological structure is known, but it is not clear in what sense the structure is optimal. In contrast, the goal of the engineering is the minimization of a given functional that is not the subject of a search; the problem is to find an unknown optimal structure. This observation reflects the principal difference between biology that seeks an answer to the question: "Why are the bio-materials and the morphology of living organisms the way they are?" and engineering that wants to know "How to make an optimal structure?" by using the biomimetics of these trees.

The structure of the paper is as follows. In the next section, we analyze the stresses in an anisotropic cylinder that models the trunk. This stress analysis considers the structure under axial loading with a bending moment. The stresses are computed as a function of the grain angle. Finally, the maximum grain angle is determined subjected to Tsai-Hill failure criteria. The objective is to determine the influence of the grain angle on the strength of the structure. The results will be applied to explain the twisting of the Ponderosa pine for verification purposes since its grain angle can easily be measured .

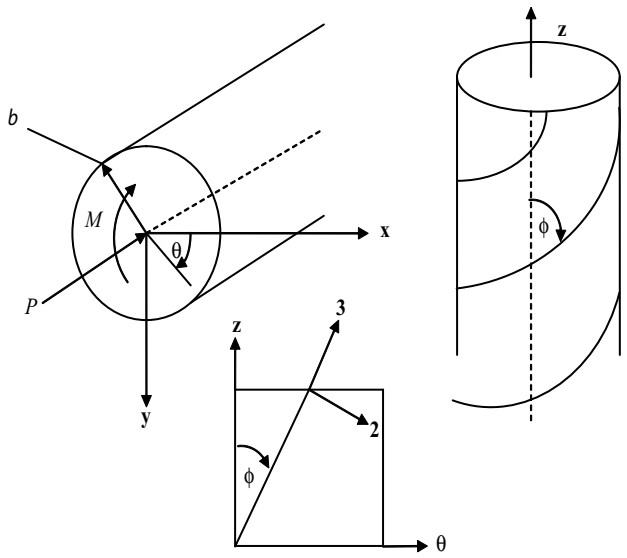

Fig. 2 Schematics of the tree trunk.

2 Analysis

Before solving for the stress fields of this structure, we give a brief overview of equations required for the computation. Consider an infinite cylinder of the radius R, fulfilled by an orthotropic linear elastic material with the compliance $\mathbf{S}$, and loaded by bending moment M and the axial load P. We want to compute the stresses and further the strength of the cylinder and trace their dependence on the angle of twist of the anisotropic fulfillment . Assume that stresses inside the cylinder satisfy equations of linear elasticity:

$$
\begin{aligned}
0 &= \nabla \cdot \boldsymbol{\sigma} \\
\boldsymbol{\sigma} &= \boldsymbol{\sigma}^T \\
\boldsymbol{\varepsilon} &= \mathbf{S} \cdot \boldsymbol{\sigma} \\
\boldsymbol{\varepsilon} &= \frac{1}{2}\left[\nabla \mathbf{u} + (\nabla \mathbf{u})^T\right]
\end{aligned}
$$

Consider differential element of the structure, the compliance of an orthotropic material can be expressed in terms of the engineering elastic parameters. In the coordinates that coincide with principle axes of anisotropy tensor (direction of the grain), the Hooke's law takes the form:

$$\varepsilon^*_{ij} = S^*_{ijkl}\sigma^*_{ij}$$

where: ε^*_{ij} are strain components, including both normal and shear, σ^*_{ij} are stress components, including both normal and shear, and S^*_{ijkl} is the compliance matrix, or in

the matrix form:

$$\begin{Bmatrix} \epsilon_{11}^* \\ \epsilon_{22}^* \\ \epsilon_{33}^* \\ \epsilon_{23}^* \\ \epsilon_{13}^* \\ \epsilon_{12}^* \end{Bmatrix} = \begin{bmatrix} \frac{1}{E_{11}} & -\frac{\nu_{21}}{E_{22}} & -\frac{\nu_{31}}{E_{33}} & 0 & 0 & 0 \\ -\frac{nu_{21}}{E_{11}} & \frac{1}{E_{22}} & \frac{\nu_{32}}{E_{33}} & 0 & 0 & 0 \\ -\frac{nu_{31}}{E_{11}} & \frac{\nu_{23}}{E_{22}} & \frac{1}{E_{33}} & 0 & 0 & 0 \\ 0 & 0 & 0 & \frac{1}{G_{23}} & 0 & 0 \\ 0 & 0 & 0 & 0 & \frac{1}{G_{13}} & 0 \\ 0 & 0 & 0 & 0 & 0 & \frac{1}{G_{12}} \end{bmatrix} \begin{Bmatrix} \sigma_{11}^* \\ \sigma_{22}^* \\ \sigma_{33}^* \\ \sigma_{23}^* \\ \sigma_{13}^* \\ \sigma_{12}^* \end{Bmatrix} \tag{1}$$

The subscript 1 represents the radial direction. Directions perpendicular and parallel to the grain are denoted by subscripts 2 and 3, respectively (see Figure 2).

2.1 Transformation of $\mathbf{S}^*$

The structure possesses cylindrical anisotropy. Hence, the analysis is conducted in cylindrical coordinates. It is needed to compute the components of (1) in the cylindrical system. The main coordinate axes of the compliance $\mathbf{S}^*$ are directed as follows:

$$\mathbf{e}_r = \mathbf{e}_1$$
$$\mathbf{e}_\theta = \cos\phi\mathbf{e}_2 + \sin\phi\mathbf{e}_3$$
$$\mathbf{e}_z = -\sin\phi\mathbf{e}_2 + \cos\phi\mathbf{e}_3$$

The new matrix can be written as:

$$\mathbf{S} = \left(\mathbf{K}^{-1}\right)^T \mathbf{S}^* \mathbf{K}^{-1}$$

where $\mathbf{S}$ is compliance matrix in cylindrical coordinates and $\mathbf{K}$ is a rotation matrix. It has a block form (Ting (1996)):

$$\mathbf{K} = \begin{bmatrix} \mathbf{K}_1 & 2\mathbf{K}_2 \\ \mathbf{K}_3 & \mathbf{K}_4 \end{bmatrix} \tag{2}$$

where

$$\mathbf{K}_1 = \begin{bmatrix} \Omega_{11}^2 & \Omega_{12}^2 & \Omega_{13}^2 \\ \Omega_{21}^2 & \Omega_{22}^2 & \Omega_{23}^2 \\ \Omega_{31}^2 & \Omega_{32}^2 & \Omega_{33}^2 \end{bmatrix}$$
$$\mathbf{K}_2 = \begin{bmatrix} \Omega_{12}\Omega_{13} & \Omega_{13}\Omega_{11} & \Omega_{11}\Omega_{12} \\ \Omega_{22}\Omega_{23} & \Omega_{23}\Omega_{21} & \Omega_{21}\Omega_{22} \\ \Omega_{32}\Omega_{33} & \Omega_{33}\Omega_{31} & \Omega_{31}\Omega_{32} \end{bmatrix}$$
$$\mathbf{K}_3 = \begin{bmatrix} \Omega_{21}\Omega_{31} & \Omega_{22}\Omega_{32} & \Omega_{23}\Omega_{33} \\ \Omega_{31}\Omega_{11} & \Omega_{32}\Omega_{12} & \Omega_{33}\Omega_{13} \\ \Omega_{11}\Omega_{21} & \Omega_{12}\Omega_{22} & \Omega_{13}\Omega_{23} \end{bmatrix}$$
$$\mathbf{K}_4 = \begin{bmatrix} L_1 & L_2 & L_3 \\ L_4 & L_5 & L_6 \\ L_7 & L_8 & L_9 \end{bmatrix}$$

and

$$\mathbf{L}_1 = \Omega_{22}\Omega_{33} + \Omega_{23}\Omega_{32}$$
$$\mathbf{L}_2 = \Omega_{23}\Omega_{31} + \Omega_{21}\Omega_{33}$$
$$\mathbf{L}_3 = \Omega_{21}\Omega_{32} + \Omega_{22}\Omega_{31}$$
$$\mathbf{L}_4 = \Omega_{32}\Omega_{13} + \Omega_{33}\Omega_{12}$$
$$\mathbf{L}_5 = \Omega_{33}\Omega_{11} + \Omega_{31}\Omega_{13}$$
$$\mathbf{L}_6 = \Omega_{31}\Omega_{12} + \Omega_{32}\Omega_{11}$$
$$\mathbf{L}_7 = \Omega_{12}\Omega_{23} + \Omega_{13}\Omega_{22}$$
$$\mathbf{L}_8 = \Omega_{13}\Omega_{21} + \Omega_{11}\Omega_{23}$$
$$\mathbf{L}_9 = \Omega_{11}\Omega_{22} + \Omega_{12}\Omega_{21}$$

Here Ω_{ij} are the elements of the matrix:

$$\mathbf{\Omega} = \begin{bmatrix} 1 & 0 & 0 \\ 0 & \cos\phi & \sin\phi \\ 0 & -\sin\phi & \cos\phi \end{bmatrix} \tag{3}$$

After the transformation, the matrix $\mathbf{S}$ takes the following form:

$$\mathbf{S} = \begin{bmatrix} a_{11} & a_{12} & a_{13} & a_{14} & 0 & 0 \\ a_{21} & a_{22} & a_{23} & a_{24} & 0 & 0 \\ a_{31} & a_{32} & a_{33} & a_{34} & 0 & 0 \\ a_{41} & a_{42} & a_{43} & a_{44} & 0 & 0 \\ 0 & 0 & 0 & 0 & a_{55} & a_{56} \\ 0 & 0 & 0 & 0 & a_{65} & a_{66} \end{bmatrix}$$

where a_{ij} are the non-zero rotated elements that are determined from (2) and (3). Stresses and strains are transformed as following:

$$\boldsymbol{\sigma} = \mathbf{K}\boldsymbol{\sigma}^* \text{ and } \boldsymbol{\varepsilon} = \left(\mathbf{K}^{-1}\right)^T \boldsymbol{\varepsilon}^*$$

where: $\boldsymbol{\sigma}$ and $\boldsymbol{\varepsilon}$ are the stress and strain in the cylindrical coordinates.

Below, stresses are analyzed for two loading cases: axial loading and bending. Due to linearity of the model, the stresses are the sum of the results from these two loadings.

2.2 Stress functions

In this analysis, the body force is neglected; the cylinder is loaded from its ends. The cylindrical coordinate system as shown previously in Figure 2 is used. It is independent of z, Thus, the equilibrium equations in cylindrical coordinates become:

$$\frac{\partial\sigma_r}{\partial r} + \frac{1}{r}\frac{\partial\tau_{r\theta}}{\partial\theta} + \frac{\sigma_r - \sigma_\theta}{r} = 0$$
$$\frac{\partial\tau_{r\theta}}{\partial r} + \frac{1}{r}\frac{\partial\sigma_\theta}{\partial\theta} + \frac{2\tau_{r\theta}}{r} = 0$$
$$\frac{\partial\tau_{rz}}{\partial r} + \frac{1}{r}\frac{\partial\tau_{\theta z}}{\partial\theta} + \frac{\tau_{rz}}{r} = 0$$

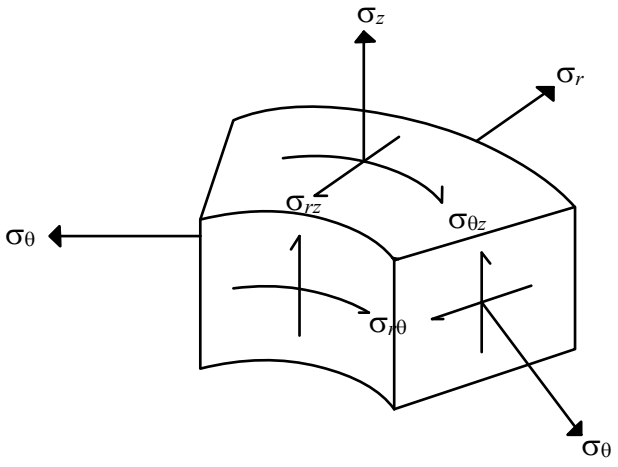

Fig. 3 Stress components in cylindrical coordinate

and

$$\sigma_z = \frac{1}{a_{33}}\left(D - a_{13}\sigma_r - a_{23}\sigma_\theta - a_{34}\tau_{\theta z} - a_{35}\tau_{rz} - a_{36}\tau_{r\theta}\right) \tag{4}$$

where (see Lekhnitskii (1981)) $D = Br\sin\theta + C$. These four equations are bound together six components of the stress tensor $\sigma_r, \sigma_\theta, \sigma_z, \tau_{\theta z}, \tau_{rz}$, and $\tau_{r\theta}$ (see Figure 3). The other coefficients, B and C are the constants that are formed from the boundary conditions. To solve for the stress fields satisfying the equilibrium equations, two stress functions $\Phi(r,\theta)$ and $\Psi(r,\theta)$ are introduced as it is common in the theory of elasticity, (see for example Lekhnitskii (1981)). The stress components are expressed through Φ and Ψ as:

$$\sigma_r = \frac{1}{r}\frac{\partial \Phi}{\partial r} + \frac{1}{r^2}\frac{\partial^2 \Phi}{\partial \theta^2}$$

$$\tau_{r\theta} = -\frac{\partial^2}{\partial r \partial \theta}\left(\frac{\Phi}{r}\right) \qquad \sigma_\theta = \frac{\partial^2 \Phi}{\partial r^2} \tag{5}$$

$$\tau_{\theta z} = -\frac{\partial \Psi}{\partial r} \qquad \tau_{rz} = \frac{1}{r}\frac{\partial \Psi}{\partial \theta}$$

Notice that σ_z is expressed through the other components by (4). According to Lekhnitskii (1981), the stress functions must satisfy the following equations:

$$L_4'\Phi + L_3'\Psi = \frac{2}{a_{33}}\left(a_{13} - a_{33}\right)\frac{B\sin\theta}{r} \tag{6}$$

$$L_3''\Phi + L_2'\Psi = \frac{2a_{34}B\sin\theta}{a_{33}} + \frac{a_{34}C}{r} - 2\xi \tag{7}$$

where L_4', L_3', L_3'', and L_2' are differential operators of the fourth, third, and second orders, respectively:

$$\begin{aligned} L_4' = {} & \beta_{22}\frac{\partial^4}{\partial r^4} + (2\beta_{12} + \beta_{66})\frac{1}{r^2}\frac{\partial^4}{\partial r^2 \partial \theta^2} + \beta_{11}\frac{1}{r^4}\frac{\partial^4}{\partial \theta^4} \\ & + 2\beta_{22}\frac{1}{r}\frac{\partial^3}{\partial r^3} - (2\beta_{12} + \beta_{66})\frac{1}{r^3}\frac{\partial^3}{\partial r \partial \theta^2} - \beta_{11}\frac{1}{r^2}\frac{\partial^2}{\partial r^2} \\ & + (2\beta_{11} + 2\beta_{12} + \beta_{66})\frac{1}{r^4}\frac{\partial^2}{\partial \theta^2} + \beta_{11}\frac{1}{r^3}\frac{\partial}{\partial r} \\ L_3' = {} & -\beta_{24}\frac{\partial^3}{\partial r^3} - (\beta_{14} + \beta_{56})\frac{1}{r^2}\frac{\partial^3}{\partial r \partial \theta^2} \\ & + (\beta_{14} - 2\beta_{24})\frac{1}{r}\frac{\partial^2}{\partial r^2} \\ L_3'' = {} & -\beta_{24}\frac{1}{r}\frac{\partial^3}{\partial r^3} - (\beta_{14} + \beta_{56})\frac{1}{r^2}\frac{\partial^3}{\partial r \partial \theta^2} \\ & - (\beta_{14} + \beta_{24})\frac{1}{r}\frac{\partial^2}{\partial r^2} + (\beta_{14} + \beta_{56})\frac{1}{r^3}\frac{\partial^2}{\partial \theta^2} \\ L_2' = {} & \beta_{44}\frac{\partial^2}{\partial r^2} + \beta_{55}\frac{1}{r^2}\frac{\partial^2}{\partial \theta^2} + \beta_{44}\frac{1}{r}\frac{\partial}{\partial r} \end{aligned}$$

and

$$\beta_{ij} = a_{ij} - \frac{a_{i3}a_{j3}}{a_{33}}$$

is the reducing strain coefficient. The derivations of these differential operators and their explicit forms are given in Lekhnitskii (1981).

2.3 Stresses due to axial loading

In the case of axial loading, the stress functions and the components of stress depend only on r. Thus, the solution to (6) and (7) are sought in the forms:

$$\Phi = f(r) \qquad \Psi = g(r) \tag{8}$$

Therefore, parameter in the right-hand side of (6) and (7) is zero. Substituting (8) into (6) and (7), the following system of differential equations are obtained:

$$\begin{aligned} 0 = {} & \beta_{22}f^{IV} + \frac{2\beta_{22}}{r}f''' \\ & - \frac{\beta_{11}}{r^2}f'' + \frac{\beta_{11}}{r^3}f' - \beta_{24}g''' + \frac{(\beta_{14} - 2\beta_{24})}{r}g'' \end{aligned} \tag{9}$$

$$\begin{aligned} & \frac{a_{34}C}{r} - 2\xi = \\ & \beta_{24}f''' + \frac{(\beta_{14} + \beta_{56})}{r^2}f' + \beta_{44}g'' + \frac{\beta_{44}}{r^2}g' \end{aligned} \tag{10}$$

We look for the solutions to the homogeneous part of (9) and (10) in the form:

$$f_h = Fr^\alpha \qquad g_h = Gr^{\alpha-1} \tag{11}$$

The subscript h denotes a homogenous solution. By substituting (11) into (9) and (10), r is eliminated, and we

obtain a system:

$$\underbrace{\begin{bmatrix} H_1(\alpha) & H_2(\alpha) \\ H_3(\alpha) & H_4(\alpha) \end{bmatrix}}_{\mathbf{H}} \begin{bmatrix} F \\ G \end{bmatrix} = \begin{bmatrix} 0 \\ 0 \end{bmatrix} \tag{12}$$

The homogeneous system has nontrivial solution F and G only if $\det(\mathbf{H}) = 0$, Solving this relation, we obtain 6 parameters for $\alpha : 0, 0, 1, 2, \alpha_5$, and α_6. The stress functions can now be expressed as:

$$\Phi = \left(m_1 + m_2 \ln r + m_3 r + m_4 r^2 + m_5 r^{\alpha_5} + m_6 r^{\alpha_6}\right) + \Phi_p \tag{13}$$

$$\Psi = \left(p_1 r^{-1} + p_2 r^{-1} \ln r + p_3 + p_4 r + p_5 r^{\alpha_5 - 1} + p_6 r^{\alpha_6 - 1}\right) + \Psi_p \tag{14}$$

where $m_1 ... m_6$, $p_1 ... p_6$ are the constants. Φ_p and Ψ_p are the particular solutions: $\Phi_p = a_1 r^3$ and $\Psi_p = b_1 r^2 + c_1 r$.

Consider the condition at point $r = 0$, one can see that $m_2 = m_3 = m_4 = p_1 = p_2 = p_4 = 0$ in order to avoid the singularity at this location. Moreover, any value of α_i that has a negative sign is discarded because stresses have to be finite. In this case, either α_5 or α_6 has a negative value. Let us assign these values to α_5, so that $m_5 = p_5 = 0$. The stress functions now become:

$$\Phi = m_6 r^{\alpha_6} + \Phi_p \qquad \Psi = p_6 r^{\alpha_6 - 1} + \Psi_p$$

The unknown constants are determined from the boundary conditions:

$$\sigma_r = \tau_{r\theta} = \tau_{\theta z} = \tau_{rz} = 0 \text{ at } r = b. \tag{15}$$

Utilizing (15), we have two equations with two unknowns. The constants in the particular solutions are determined from the end conditions:

$$\int_0^b \sigma_z r dr = \frac{P}{\pi b^2} \qquad \int_0^b \tau_{\theta z} r^2 dr = 0$$

where P is the axial loading and b is the radius of the cylinder. Once all the constants are determined, stress components can then be evaluated according to (5). Because of the spiral anisotropy, the axial loading causes the cylinder to twist. The displacements are not computed in this analysis, since the main objective is to determine the stresses.

2.4 Stresses due to bending

Let us analyze the case where the structure is in pure bending. A bending moment M is applied at each end (Figure 2). The analysis still follows the same procedures as in axial loading case with the different stress functions:

$$\Phi = f(r) \sin\theta \qquad \Psi = g(r) \sin\theta$$

In the pure bending case C and ξ in (6) and (7) are zero. Substituting the above stress functions into (6) and (7), the following systems of differential equations are obtained:

$$\frac{2\left(a_{13} - a_{33}\right) B}{a_{33} r} = \beta_{22} f^{IV} - \frac{(2\beta_{12} + \beta_{66})}{r^2} f'' + \frac{\beta_{11}}{r^4} f + \frac{2\beta_{22}}{r} + \frac{(2\beta_{12} + \beta_{66})}{r^3} f' - \frac{\beta_{11}}{r^2} f'' - \frac{(2\beta_{11} + 2\beta_{12} + \beta_{66})}{r^4} f + \frac{\beta_{11}}{r^3} f' - \beta_{24} g''' + \frac{(\beta_{14} + \beta_{56})}{r^2} g + \frac{(\beta_{14} - 2\beta_{24})}{r} g'' \tag{16}$$

$$\frac{2 a_{34} B}{a_{33}} = - \beta_{24} f''' + \frac{(\beta_{14} + \beta_{56})}{r^2} f' - \frac{(\beta_{14} + \beta_{24})}{r} f'' - \frac{(\beta_{14} + \beta_{56})}{r^3} f + \beta_{44} g'' + \frac{\beta_{55}}{r^2} g + \frac{\beta_{55}}{r^2} g' \tag{17}$$

Similar to the axial loading case, the solutions to the homogeneous part of (16) and (17) assume the forms of (11), and α is solved as described in the axial loading case using (12). Solving (12) yields six values 1, 1, α_3, α_3, α_4, α_5, and α_6. Their expressions are shown in Appendix. The stress functions can now be expressed as

$$\Phi = \left(m_1 r + m_2 r \ln r + m_3 r^{\alpha_3} + m_4 r^{\alpha_4} + m_5 r^{\alpha_5} + m_6 r^{\alpha_6}\right) \sin\theta + \Phi_p$$

$$\Psi = \left(p_1 + p_2 \ln r + p_3 r^{\alpha_3 - 1} + p_4 r^{\alpha_4 - 1} + p_5 r^{\alpha_5 - 1} + p_6 r^{\alpha_6 - 1}\right) \sin\theta + \Psi_p$$

where $\Phi_p = a_1 r^3 \sin\theta$ and $\Psi_p = b_1 r^2 \sin\theta$. Once again, by setting the condition at $r = 0$, one can see that m_2 and p_2 are zero, and as in the axial loading case, any value of α_i that has a negative sign is omitted. Now, the stress functions become:

$$\Phi = \left(m_3 r^{\alpha_3} + m_4 r^{\alpha_4}\right) \sin\theta + \Phi_p$$

$$\Psi = \left(p_3 r^{\alpha_3 - 1} + p_4 r^{\alpha_4 - 1}\right) \sin\theta + \Psi_p.$$

The unknown constants m_3, m_4, p_3, and p_4 are determined from the boundary conditions:

$$\sigma_r = \tau_{r\theta} = \tau_{\theta z} = \tau_{rz} = 0 \text{ at } r = b. \tag{18}$$

Utilizing (18), a system of four equations and four unknowns is obtained. The constants in the particular solutions are determined from the end conditions:

$$\int_0^{2\pi} \int_0^b \sigma_z r^2 \sin\theta dr d\theta = M$$

$$\int_0^{2\pi} \int_0^b \sigma_z r^2 \cos\theta dr d\theta = 0.$$

Finally, stress components can then be evaluated according to (5). This computation was carried out using Maple V. This analysis enables us to compute stresses in an anisotropic elastic cylinder with rotated axes of anisotropy. Although the calculations are analytic, the resulting formulas (obtained by Maple V) are bulky and we do not display them here.

2.5 Failure criteria

Due to the nature of the anisotropy, the conventional maximum strength criterion for isotropic materials gives a poor prediction of failure (Swanson (1997)). For wood, we use Tsai-Hill failure criterion:

$$\left(\frac{\sigma_1}{\sigma_{1u}}\right)^2 + \left(\frac{\sigma_2}{\sigma_{2u}}\right)^2 - \frac{\sigma_1\sigma_2}{\sigma_{1u}^2} + \left(\frac{\tau_{12}}{\tau_{12u}}\right)^2 < 1 \qquad (19)$$

When the left hand side of (19) is greater than or equal to 1, the failure is predicted. No distinction is made between compressive and tensile stresses.

Another criterion that is often used for wood structure is Hankison's formula (Gedney (1986)):

$$\sigma_u = \frac{\sigma_{1u}\sigma_{2u}}{\sigma_{1u}\sin^2\phi + \sigma_{2u}\cos^2\phi}$$

Hankinson's formula approximates the ultimate axial strength as a function of the grain angle.

3 Analysis of Ponderosa pine

Based on the pure mechanical model presented in the previous section, the stresses were determined for Ponderosa pine. First, the stresses were computed for the case of axial loading and then the case of a bending moment. The computation of stresses demonstrates whether spiraling is related to the elastic properties of the tree. If nature has already optimized the structure of living organisms, one expects the structure of the tree be optimized for the environment surrounding it. For instance, the structure of the tree should be in the configurations that maximize its strength to support the weight of branches, leaves, snow, and also resistance to the wind.

3.1 Setting of the parameters

We assumed that the trunk of the Ponderosa pine is cylindrical with radius $r = 10$ in. In addition, the axial loading is only a result of the weight and has the magnitude $P = 1500$ lb. The bending moment is approximated to be 10000 lb·in from the wind force. All the parameters are approximated in English unit in order to apply directly to the data that were obtained for Ponderosa pine. Table 1 shows the properties of the Ponderosa pine (Bodig and Jayne (1996)). Material strengths are (The Forest Products Laboratory (1955)): $\sigma_{33t} = 6300$ psi, $\sigma_{33c} = -5270$ psi, $\sigma_{22t} = 400$ psi, $\sigma_{22c} = -740$ psi, $\tau_{23ul} = 1160$ psi.

Table 1 Elastic moduli of Ponderosa pine with 12 % moisture content, 106 psi.

E_1	E_2	E_3	G_{12}	G_{13}	G_{23}
0.1236	0.0743	1.423	0.00994	0.1035	0.0978

Utilizing this information, the calculation of stresses was performed. In this case, if the spiral angle is less than 21.2°, some α's in (13) and (14) become negative. This leads to singularity at the center of the trunk at which $r = 0$. As a result, we only look at the grain angle ϕ that varies from 21.2° to 90°. Applying (19), we can predict when the structure fails.

3.2 Results

Figure 4 shows the total stresses resulting from bending and axial loading. Here, we look at the stresses and the maximal grain angle of Ponderosa pine using data and criteria given in Section 3.1 and Section 2.5. In addition, stresses are only investigated on the surface at $\theta = 90°$ and $\theta = -90°$ because maximum compressive and tensile stresses are expected at these locations. Only the plots of the stress fields are illustrated due to the size of the stress equations. Since P and M were arbitrary chosen, it is interesting to see how the failure prediction would vary if P or M changes. It is appropriate to vary M since the speed of the wind varies more than the weight on top of the tree. The grain angle and the Tsai-Hill minimum failure values are shown in Figure 5.

As the magnitude of the bending moment increases, the maximal grain angle becomes smaller in order to reduce the bending stress. Maximal grain angle is approximately 37° (Figure 5). At this grain angle, the Ponderosa pine fails when the magnitude of the bending moment increases to 800 kip·in. Naturally, trees are uprooted when wind load is high. The stresses produced by the wind load in nature are not typically high enough to exceed the strength of this tree. The ultimate strength of the Ponderosa pine is shown in Figure 6 using Hankinson's formula and Tsai-Hill failure criterion.

4 Structural optimization

In the beginning, we mentioned that the spiraling allows the fluid to be transferred throughout the whole

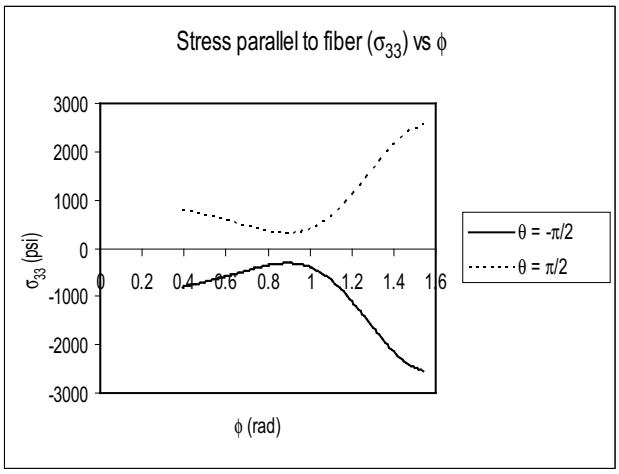

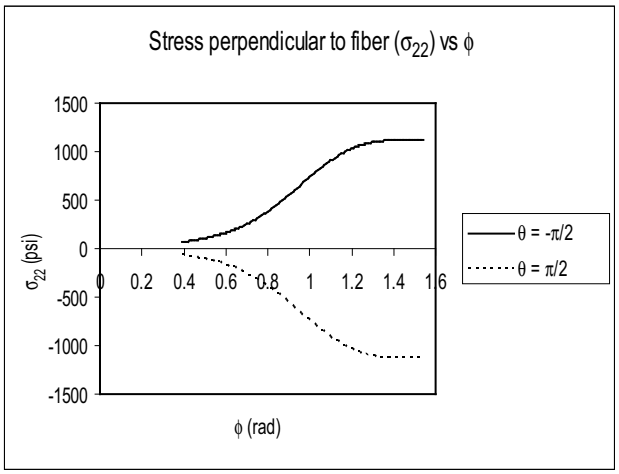

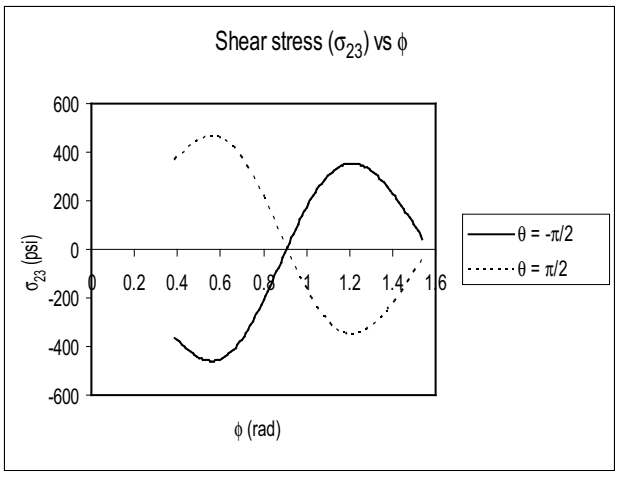

Fig. 4 Total stresses on the surface of the tree.

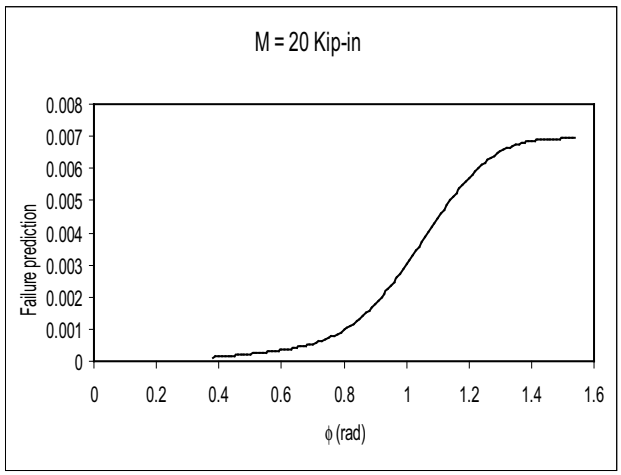

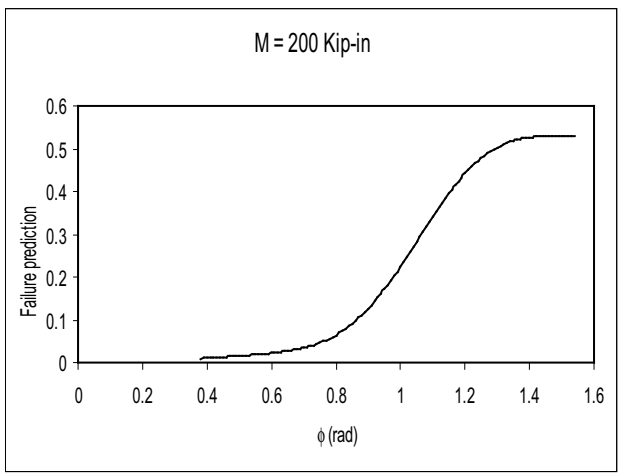

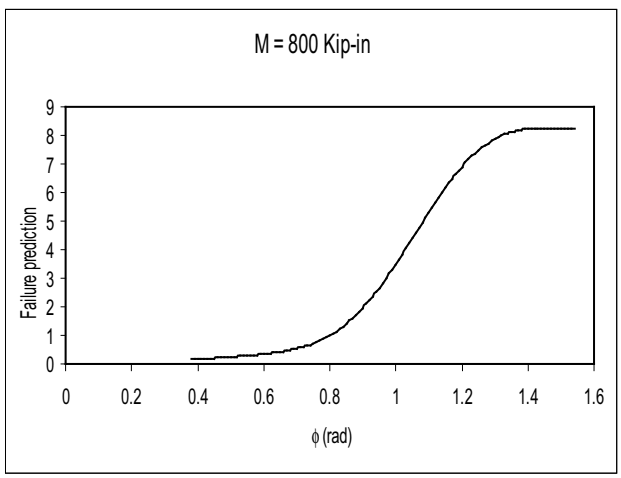

Fig. 5 Failure prediction using Tsai-Hill criterion at $\theta = \frac{\pi}{2}$.

tree even though if the roots on one side has died. However, the presence of the spiraling also causes the tree to become less stiff. Hence, we need to determine the maximum grain angle that does not affect the strength of the tree significantly.

Having obtained the results of the failure predictions, one may use them to gain the benefits of the biomimetics of these trees. From Figure 5, we can see that the curves from these plots have the same shape but with the different in magnitudes. These curves show that there is a sharp increase in magnitude beyond 37°. From this observation, one could set up the problem of finding maximum angle as a problem of optimization with constraints as following:

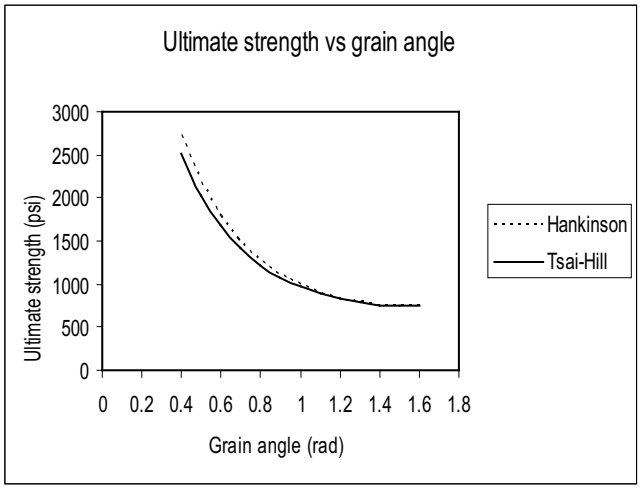

Fig. 6 Ultimate strength of Ponderosa pine at various spiral angles.

Maximize the angle ϕ ($0 \leq \phi \leq \frac{\pi}{2}$) subject to the conditions

1. Failure criterion is satisfied (19)
2. Parameters of materials and loadings are as described in Section 3.1
3. The angle ϕ is within the range preceding the point where the sharp increase of the slope in Figure 5 takes place.

5 Discussion and conclusions

From this analysis, one cannot fully explain the relationship between the spiral twist and the mechanical properties of the tree; it is more reasonable to assume that the spiraling has to deal with fluid transportation that we mention in the introduction. Instead, it might be more appropriate to ask how big the angle could be in order for the tree to still remain strong. Excessive spiraling not only reduces the stiffness of the tree but also weakens the strength of the tree. Hence, there ought to be a limiting point on how much the stiffness can be reduced in order for a tree to stand up straight. Its chance against breaking would increase if the tree does not bend much.

The result from Figure 5 shows that the failure prediction value increases slowly to about 37°, and then the slope increases dramatically beyond this point. The tree strength is not sacrificed considerably, as long as the grain angle remains below 37°. The grain angle of the Ponderosa tree obtained using theory of anisotropic elasticity is slightly different from the angle measured in the Figure 7. However, this was expected since many assumptions were made during the analysis. The permitted interval according to this analysis is between 21.2° and 37°.

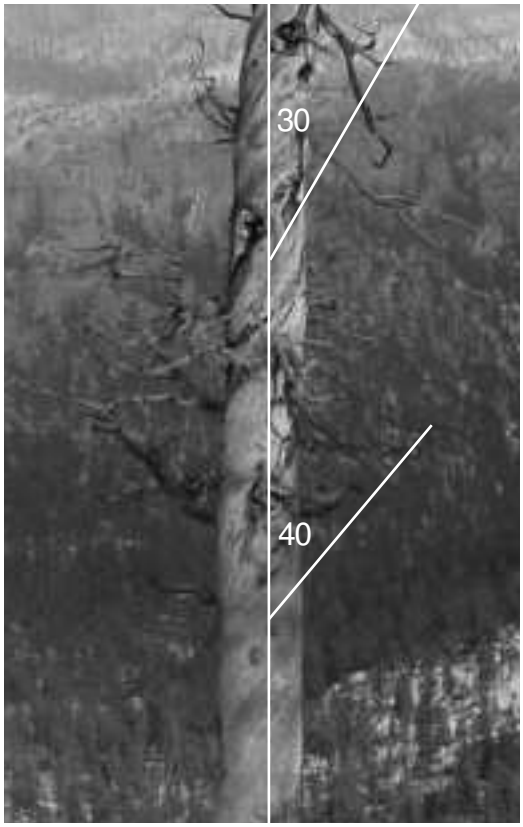

Fig. 7 Angle measurements at the lower and upper portion of the trunk.

Another observation that was made was the differences between the lower and the upper portion of the tree (Figure 7). The grain angle is a little bigger toward the bottom. When the tree is small, it requires more distribution of fluid to ensure proper growth. Having the fiber spiral at a bigger angle allows the tree to receive more fluid along its circumference. As the tree grows taller, the angle becomes smaller, which allows the fluid to be transported to the higher portion faster by reducing the coverage area. This could be another reason why the grain angle varies this way. Details about the fluid transportation are not discussed here since it is beyond the scope of this analysis.

We did not consider the cracking of the trunk in this analysis. Meanwhile, this may be an important factor. Looking at the elastic constants of this tree, one finds that E_2 is approximately 5% of E_3, which is almost as there is a crack. With this in mind, Leonid Slepyan (via private communication) has pointed out that, as the crack wiggles around the tree, it is less prone to fracture than when the crack is vertically straight.

Due to lack of information and actual data, average wind load and the load that can uproot the Ponderosa tree, it is not possible to give a solid conclusion regarding relationships between the magnitude of the twist and the elastic properties of trees. In addition, the results presented in this analysis only reflect the Ponderosa pine.

Our analysis shows that the problem of adaptation of a tree' trunk can be viewed as a problem of constrained minimization. The spirals in the grain are developed for the non-mechanical reason (transport of the water to branches) and the strength analysis provides a constraint that limits the angle of these spirals. Namely, we observe that the strength is practically the same for the angles that do not surpass the critical value, and this critical value is what we see in Nature. In short, a structure can be more flexible by having the fibers spiral along its circumference. However, depending on the elastic properties of the material, the angle of the spiral can vary.

6 Acknowledgements

We are indebted to many people that encouraged us and advised us on different aspects of the modelling and analysis. Their general comments and suggestions were sound and worthwhile. Particularly, we mention the help from Tim Folias, Stephen Swanson, Leonid Slepyan, Steve Cowin, Jack H.T. Chang, and Natalya Kizilova. One special thanks to Roderic Lakes, who offered numerous suggestions on the first draft. The problem was presented for discussion on our website http://www.math.utah.edu/ cherk, and we enjoyed numerous comments from colleagues, whom we are thankful. The work was sponsored by National Science Foundation (NSF Grant No: DMS- 0072717).

References

Bodig, J. and Jayne, B. A., *Mechanics of Woods and Wood Composites* (Van Nostrand Reinhold, New York 1982)

The Forest Products Laboratory, *Wood Handbook, No. 19* (U.S. Department of Agriculture, Washington, D.C.) 76

Gedney, L., Alaska Science Forum **Art 783**, (1986).

Kubler, H., Trees **5**, (1991) 125-135.

Lekhnitskii, S. G., *Theory of Elasticity of an Anisotropic Body* (MIR Publishers, Moscow 1981)

Swanson, S. R., *Introduction to Design and Analysis with Advanced Composite Materials* (Prentice-Hall, New Jersey 1997)

Ting, T. C. T., *Anisotropic Elasticity: Theory and Apppli-cations* (Oxford University Press, New York 1996)